Detection of radioactive gas with scintillating MOFs

Sharvanee Mauree, Vincent Villemot, Matthieu Hamel, Benoit Sabot, Sylvie Pierre, Francesca Belloni, Christophe Dujardin, A. Comotti, J. Perego, S. Bracco, et al.

Technical papers

Detection of radioactive gas with scintillating MOFs

Sharvanee MAUREE[1¥], Vincent VILLEMOT[1¥], Matthieu HAMEL[1], Benoit SABOT[2], Sylvie PIERRE[2] Christophe DUJARDIN[3], Francesca BELLONI[1] Angiolina Comotti[4], Silvia Bracco[4], Jacopo Perego[4], Guillaume H. V. BERTRAND[1]*

[1] Université Paris-Saclay, CEA, List, F-91120, Palaiseau, France

[2] Université Paris Saclay, CEA, List, Laboratoire National Henri Becquerel (LNE-LNHB), F-91120 Palaiseau, France

[3] Institut Lumière-Matière, CNRS UMR5306, Université de Lyon 1, 69622 Villeurbanne CEDEX, France

[4] University of Milano – Bicocca, Department of Materials Science, Via R. Cozzi 55, 20125 Milan, Italy

Commenté [EH1]: ORCID si possible à rajouter : 0000-0002-3499-3966

Commenté [BG2]: https://orcid.org/0000-0003-3043-8006

Commenté [BG3]: 0000-0003-2061-9241

Abstract

Homogenous radioactive gas contamination constitutes the hardest challenge for radioprotection and measurements due to the elusive nature of its origin. The three main components of this contamination are ^{85}Kr, ^{222}Rn, and tritiated (^{3}H) vapors (HT or HOT). Each of them has different issues and applications, often leading to specialized and single-gas detectors. The state of the art in terms of detection efficiency is either first liquid scintillation counting that produces chemical-radiological waste and is hard to implement online, then large ion diffusion chamber that requires large volume (> 5 L) to achieve low detection threshold. We present here an applied new paradigm to radioactive gas detection that can virtually be employed for any gas, can perform online detection and can fit in the hand. The core of our approach resides in the use of photoluminescent Metal Organic Frameworks (MOFs) as both porous gas sponges and scintillators. We synthesized, characterized, and studied the response of MOF-5, MOF-205, IRMOF-9, and a MOF-5 doped with anthracene. Using a unique technique in the world radioactive gas test-bench, we show that these MOFs present remarkable properties, achieving successful detection of ^{85}Kr, and demonstrating their ability to concentrate the radioactive gas inside their pores. We furthered our investigation with ^{85}Kr demonstrating the reproducibility of our system and even calibrating it with a range of different activities, going as low as 35 $Bq \cdot cm^{-3}$, with room for improvements. We then successfully show that our two best MOFs were able to detect ^{222}Rn and its daughter isotopes with the observation and measurement of its half-life. Finally, we completed our study with a successful detection of tritiated dihydrogen commonly known to be a hard radionuclide to detect due to its low energy and penetration range. This paper shows that scintillating MOFs are a powerful solid-state approach and a practical solution to the challenge of radioactive gas measurements.

¥ These authors have contributed equally.

¥ These authors have contributed equally.

Introduction

In the field of nuclear detection, airborne contamination represents a very specific challenge. As opposed to liquid or solid state contamination, radioactive gases are a more elusive danger as their volatile nature makes them more challenging to contain. Because of its volatile nature, online detection is also of paramount importance to mitigate exposure. Airborne contamination can be categorized as either heterogeneous (aerosols) or homogeneous (mainly noble gas and tritiated gas). Heterogeneous contaminations are commonly captured with a filtration technique. It aims at depositing and concentrating the suspended contamination on a filter, thus obtaining a solid state radioactive source, which is then measured by a classical contamination meter[1,2]. Homogeneous contaminations are impervious to this technique and need a dedicated solution. Very few technologies are able to efficiently perform such a detection[3–5] , and this is our focus here. To encompass this field, we will present here the three "usual suspects" of airborne homogeneous contamination and the challenge they each represent.

^{85}Kr is a noble gas, which is a quasi-pure beta emitter (99.7% beta) with an average energy of 251 keV and a maximum at 687 keV. ^{85}Kr represents the majority of the manmade airborne contamination, as it is part of the nuclear fuel reprocessing cycle[6] . Its emissions are estimated at 379 PBq/year for the La Hague reprocessing plant in 2019 and 95 PBq/year for Sellafield reprocessing plant in 1999[7]. To the best of our knowledge, these two reprocessing plants are the only ones that have quantified their emissions, so these are bottom values that stress out the need for a suitable detector able to monitor the exposure to ^{85}Kr in these working environments. The order of magnitude of ambient radioactivity in these facilities depends on the location: 1 kBq·cm^{-3} at the mouth of the evacuation chimney as opposed to the 1 Bq·cm^{-3} at the ground level of the facility and to the natural occurrence of 1 Bq·m^{-3}. Furthermore, ^{85}Kr is a classical fission product present in the atmosphere of nuclear power plants, especially in the nuclear core building. The level recommended by the european commission and by EDF (French electricity provider who run the nuclear power plants park) in reactor building [8] is 1.8 Bq.cm^{-3}. Continuous monitoring of ^{85}Kr concentration is not yet implemented due to the lack of an online detector able to sense these levels. Still, such an apparatus could be of paramount importance in the radioprotection of workers as well as an indicator of the core's structural health.

^{222}Rn is a noble gas and an alpha emitter of 5.59 MeV. It makes for the large majority of natural homogenous airborne contamination, as ^{222}Rn is a daughter isotope of the ^{238}U decay chain. In regions with granitic bedrock, its accumulation in closed rooms and underground is a real public health problem. ^{222}Rn is evaluated to be the second cause of lung cancer behind tobacco consumption[9]. World Health Organization (WHO) and the European Commission set a guideline level of 400 Bq·m^{-3} for existing houses and 200 Bq·m^{-3} for future dwellings [10]. As an alpha emitter, detection of radon cannot be performed at distance, due to its low penetrating power. This low range makes planar scintillator not suitable for the job, and, as tritium below, emphasizes the need of a volume detection. Reaching low detection level is not straightforward in classical configuration (i.e either with direct or indirect detection with simple geometries)

^{3}H (tritium) can be present as tritiated dihydrogen or tritiated water vapor. It is a pure beta emitter with an average energy of 5.7 keV and a maximum at 18.6 keV. This very low energy makes it very difficult to detect, as its maximum penetration is only 6 mm in air and 6µm in water. This strong screening effect of the carrier gaz makes most traditional sensors inefficient with a poor effective gas volume of detection. Tritium is present in different applications; it is an activation product of the nuclear fuel cycle, the primary fuel for fusion reactors (ITER) and bombs. Its detection presents both civilian and military applications [11,12] .

Outside of these three gases, other isotopes of interest are ^{133}Xe (pulmonary imaging) and ^{135}Xe (fission product), which have beta emission between ^{85}Kr and ^{3}H; other isotopes of radon are also interesting but very close to ^{222}Rn in term of decay chain. This reinforce our approach as this marginal gas decay mode are comprise in the range we are studying.

As shown above, there are no common applications, sources, or even decay modes for each of these radioactive gases. The state-of-the-art solution for radioactive gas detection is therefore application-driven. One can find very specialized detection devices, such as diffusion chambers with membranes, which isolate radon from the air, but for radon measurement only. The two best available technologies that could be flexible are proportional gas counters[5] and liquid scintillation counting[3]. Proportional gas counters can offer online detection but need a carrier gas, which is often argon-methane (explosive) or xenon (expensive). They often use oxygen exclusion technics as it diminish performance of the detectors, adding an O_2/N_2 separation apparatus to the detector. Furthermore, the counting system is quite imposing, and the need for gases adds a very bulky pressurized bottle to the setup, making it a stationary-only solution. Liquid scintillation is best for low penetrating ionizing rays. It is the metrological standard for alpha emissions from ^{222}Rn (thanks to radon solubility in liquid scintillator) or weak beta from tritium. However, it is not possible with ^{85}Kr due to its poor solubility in liquid scintillator. The use of a liquid scintillator comprises a sampling step to dissolve the gas in a material (bubbling in water, absorption on material), making this technique impractical for online measurements and not fully reproducible due to the volatility of noble gas in the liquid scintillator. Each liquid scintillation measurement also produces liquid waste with mixed hazards, chemical and radiological, that are difficult to dispose of.

There is a real need for very sensitive detectors able to perform online measurements of radioactive gas. The solution we propose herein is inspired by the efficiency of the liquid scintillator regarding its interaction with a radionuclide. We can conceptualize it as similar to a radionuclide in solution, which has a maximum surface in contact with the scintillator, avoiding the self-shielding of low beta or alpha emitter. We thus turned our attention to materials with very high specific areas that interact optimally with gases and exhibit scintillating properties. Metal Organic Frameworks (MOFs) stand out as one of the ideal solutions for this problem as they are the class of materials with the highest specific surfaces and can be chemically designed almost at will. The core idea of our approach is to use all the remarkable features of MOFs to our advantage, since they can be both the scintillator (radiation detection) and a radioactive gas sponge[13], with the possibility of adsorbing, concentrating/selecting and detecting the targeted gas. MOFs for radiation detection have already been explored in the literature [14–16] as scintillators dispersed in polymeric matrices[17–19], very much to the style of plastic scintillators. Their potential as both radioactive gas sponge and scintillators was theorized[20] but never explored together. In this paper, we are proposing to take this step, demonstrating all the potential of scintillating MOFs for radioactive gas detection. We first synthesized four MOFs with complete structural and photophysical characterization. Then we recorded their scintillation properties in the presence of radioactive gas. To do so, we placed the MOFs inside a metrological device, a triple-to-double coincidence ratio (TDCR) counter[21], modified to be connected to a metrological radioactive gas test bench[22]. We showed that scintillating MOFs are an extremely potent solution for the detection of medium level (35 to 250 $Bq \cdot m^{-3}$) of our targeted radioactive gases. This first evaluation of performances, in terms of detection threshold and response time, makes the use of MOFs already a game changer in the field of radioactive gas detection.

Method

Our approach for radioactive gas detection is based on the combination of porosity and photoluminescence in MOFs. In order to achieve this duality, we focused on the synthesis of known MOFs with classical structural characterization for the porosity aspect (PXRD, BET, TGA). We also performed photophysical as well as radiophysical experiments on each of them to evaluate their properties. All the characterization can be found in the supporting information.

As our main focus and innovation is radioactive gas detection, we will present here our homemade metrological test benches. The gas bench consists of various mixing lines allowing the dilution of primary radioactive gas standards and their easy handling[22] . This installation enables us to produce samples whose total activity is controlled and known precisely for any radioactive gas except ^{222}Rn, which has another dedicated setup[23]. These samples are then connected to a closed circuit (total volume of 139 cm^3), allowing the production of a radioactive atmosphere of known activity in dry, filtered air (i.e. without aerosols and relative humidity < 3 %). Two identical experimental setups (Figure 1) were designed, one for ^3H (contaminating gas) one for the other radioactive gases; they consist of:

- a container (**1**) with a volume of 104.4 (5) cm^3 capable of containing a known activity of radioactive gases;
- a pump (**2**) allowing gas circulation in the system at a rate of 0.70 (5) $L \cdot min^{-1}$, providing a homogenous distribution of radioactive gas in the circuit within seconds;
- a TDCR counter with a circulation vial (**3**) and its associated electronics (**4**);
- a clean air inlet and outlet (**5**) to purge the system.

The TDCR counter is a precise metrological device, which consists of three photomultiplier tubes (PMTs) and allows absolute activity measurement of alpha, low-energy beta, and electron-capture radionuclides with liquid scintillation samples[24] . This system, micro-TDCR, was developed and built at LNE-LNHB and was validated and used for various studies over the last 5 years[25] . This micro-TDCR uses 3 PMTs with a maximum quantum yield (43%) between 280 nm and 420 nm. This measurement set uses specific electronics, which allows to record the logical sum of the double coincidences (*D*) as well as the triple coincidences (*T*) between the three PMTs with an adjustable coincidence window (here 40 ns or 400 ns) and an extendable dead time of 50 µs. For the first time, the TDCR device was adapted as a circulating device to accommodate a vial with a tube in the center containing the MOF crystals. This tube was reduced to an internal diameter of 4 mm to limit light scattering from the sample and thus collect maximum information using the three PMTs.

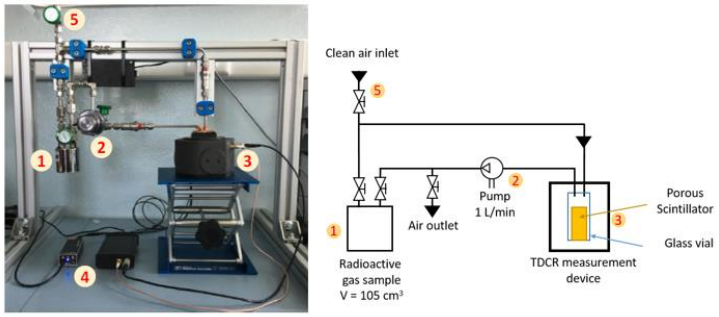

Figure 1: Top: Primary radioactive gas test bench for the generation of metrological control gas sample. Bottom left: Photo of the miniaturized radioactive gas test bench. Bottom right: Schematic representation of the system (not to scale).

For each experiment, the same type of sequence was carried out; the duration of each step was adapted according to the phenomena observed during the experiment (stable count rate, yield evolution, possible absorption....). These experimental sequences were divided into three steps:

- Measurement of a reference blank: circulation of clean air without additional radioactivity,
- Circulation of radioactive gas sample (^{85}Kr, ^{222}Rn or ^{3}H), only one isotope mixed with air, into the vial with the scintillator, the targeted activity of the sample is 10 kBq corresponding to a high activity concentration of 72 $Bq{\cdot}cm^{-3}$ in the loop,
- Circulation of clean air into the device to purge the radioactive gas.

During the whole experiment, we followed the logical sum of the double coincidence counting rate (*D*) of the TDCR device. This *D* value can be observed at two different coincidence windows, 40 ns or 400 ns. We also measured the triple coincidence (*T*) and deduced the efficiency indicator (*T/D*), which in a perfect case has a value of 1, meaning 100% detection efficiency. From these results, we can deduce if we have radioactive gas detection, its detection efficiency, adsorption, desorption, or other phenomena.

To explore the capacity of MOFs to efficiently interact with radioactive gas, the MOFs were activated under vacuum and temperature before being placed inside the experiment vial. Our best candidates were also characterized more thoroughly with the help of solid-state and hyperpolarized Xenon NMR.

Result and discussion

Scintillating MOFs library

Fluorescent MOFs are widely known in the literature[26–28], and numerous ligands used in these MOFs are also found in classical organic scintillators[29,30]. We focused our synthetic efforts on MOFs containing aromatic conjugated structures (Table 1). We chose as a baseline MOF the iconic MOF-5, which can exhibit a fluorescence between 350 nm and 450 nm depending on its hydration state[31] . We then extended toward the iso-reticular structure with MOF-9, a concatenated MOF based on a biphenyl unit. MOF-205 was also synthesized, as it is a two-ligands system based on a triphenyl benzene and a naphthalene building blocks. The latter is very interesting as it is often used in liquid scintillators for its photophysiques characteristic (decay time, wavelength, quantum yields, …).

We also explored a last avenue to make scintillating MOFs: partial ligand doping. As described in the literature[32] it is possible to replace small quantities of a ligand with another sharing the same size and chelating groups. This is a way to introduce distinct ligands in a stable but poorly fluorescent lattice in order to improve the optical properties of known MOFs without altering their structures. Hence, we synthesized and tested MOF-5 derivatives doped with 9,10-anthracene dicarboxylic acid (ADC), named here MOF-5-ADC.

Table 1: MOFs used in this study.

MOFs names	*Ligand(s)*	*Nodes*	*SI References*
MOF-5	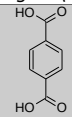	Zn_4O	Fig. S2 – S9
MOF-9	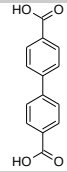	Zn_4O	Fig. S10 – S16
MOF-205	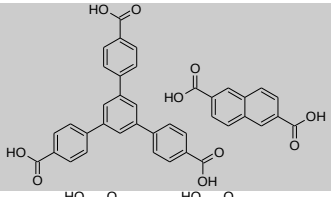	Zn_4O	Fig. S17 – S25
MOF-5-ADC	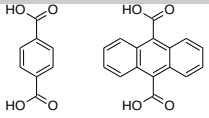	Zn_4O	Fig. S26 – S34

Photophysical characterization

Each of the synthesized MOFs was targeted because of their fluorescence properties. All these analyses are available in the SI, but we will present here the case of our doped MOF. MOF-5 is an iconic material that is easy to produce and has known fluorescence properties[31] that depend on its hydration level and structural integrity. Pure anhydrous MOF-5 has a very low fluorescence yield and an emission centered at 350 nm (FWHM ≈ 100 nm). The insertion of a small percentage (1.34 %) of 9,10-anthracene dicarboxylic acid in its lattice reminds us of the standard strategy with plastic scintillators to dope a styrene matrix with efficient fluorophores[29].

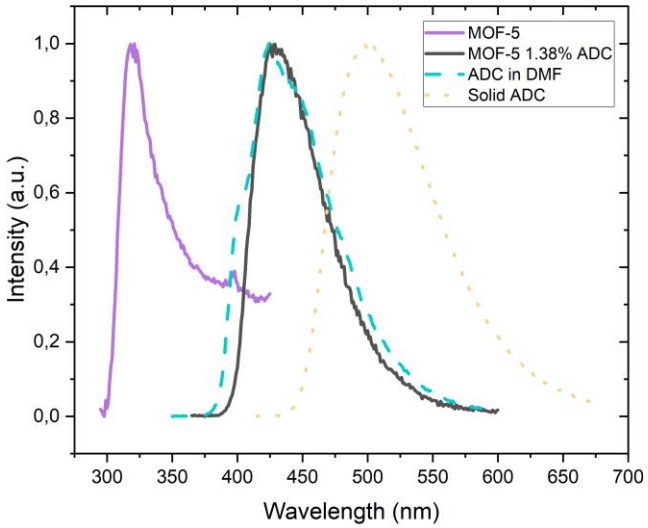

Figure 2: Photoluminescence spectra of MOF-5 and MOF-5 doped with ADC, and its comparison with ADC as a solid or in solution

In Figure 2, we present the photoluminescence (PL) and PL-excitation (PLE) spectrum of undoped and doped MOF-5. The effect of this doping is such that it is clearly visible with the naked eyes: the shift of the wavelength and the increase in light yield are visible in Figure 2. This emission wavelength of MOF-5-ADC is more suited for scintillation set-up, as traditionally, PMTs have a maximum efficiency around 420 nm. Each MOF was also tested in a radioluminescence experiment with X-rays as the excitation source, and the results are also presented in the ESI.

MCNP-6 Simulation

Monte-Carlo simulation was performed to evaluate the proportion of beta decay from ^{85}Kr that escaped from our sample container without interacting with the MOF, and are detailed in the SI.

Solid state and Xenon NMR experiments

A prescreening was realized and showed that MOF-205 and MOF-5-ADC are our most promising candidates for detection of radioactive gases. Powder XRD of the activated MOF-5-ADC and MOF-205 show high crystallinity and profiles corresponding to the known crystal structures, as observed by the comparison of the experimental to the calculated powder patterns and according to their cubic structures with space groups Fm-3m and Pm-3n, respectively [33,34] . The cubic crystal structure of MOF-5-ADC comprises octahedron-shaped Zn_4O clusters as secondary building units, connected by terephthalate ligands, thus forming intercommunicating cavities. MOF-205 is constructed by two distinct ligands, trifunctional tris-carboxybenzyl-benzene and bifunctional dicarboxylate naphthalene, which are coordinated with Zn_4O cluster and contain dodecahedral and tetragonal interconnected pores.

^{13}C MAS experiments confirm the stoichiometry of the MOFs and the absence of any signal which could pertain to residual solvents. ^{13}C CP MAS NMR spectra of MOF-5-ADC show three narrow signals according to the ligand structure and symmetry whilst MOF-205 CP-MAS NMR spectra display two resonances at about 175-176 ppm assigned to the carboxylate groups of the two ligands and a multiplicity of signals in the aromatic region in agreement with the independent carbon atoms in the unit cell. The fully relaxed 13C MAS NMR spectrum of MOF-205, collected with 60s recycle delay between pulses, confirms the relative ratio of the two ligands (2:3 trifunctional vs difunctional-based ligands) in the crystal structure.

Porosity of both MOFs samples was tested by N_2 adsorption isotherms at 77 K. The results show high surface areas of 3752 (Langmuir) and 3344 $m^2 \cdot g^{-1}$ (BET) for MOF-5-ADC and 5390 (Langmuir) and 4350 $m^2 \cdot g^{-1}$ (BET), which are among the best values published for this MOFs.[33,34] . Pore size distribution, as calculated by Non Linear DFT and carbon slit pore model, was centered at 12.5 Å for MOF-5-ADC whilst two maxima at 13.5 Å and 17.3 Å were observed for MOF-205, in agreement with the pores predicted by the crystal structures.

The accessibility of the pores to the gas phase under a flow of a noble gas such as Xe was demonstrated by Continuous Flow Hyperpolarized (CW-HP) ^{129}Xe NMR, which is a laser-assisted technique enabling to detect a signal of the diffused gas into the cavities at high resolution. The optical pumping technique allows to achieve high sensitivity (hundreds of times the signal intensity detected under thermal conditions) even with a low 1-2% concentration of xenon in a gas mixture with 94% He and 4% N_2. [35,36]. The experiments, performed at low partial pressure, ensure that intermolecular interactions of xenon with the framework prevail, while Xe-Xe interactions are negligible. Thus, the xenon chemical shifts depend only on the distinct environments of xenon confined into the restricted spaces. Remarkably, such signal can be observed after only a few ms (< 200 ms) after the contact of the gas with the porous materials. Notably, the CW-HP ^{129}Xe NMR spectra of the two MOFs at room temperature show two predominant signals in the region at about 50 ppm for MOF-5-ADC and 45 ppm for MOF-205 that are different from the free gas (at 0 ppm), indicating a fast diffusion of xenon atoms in the confining cavities. The downfield resonances demonstrate that xenon atoms are interacting with distinct adsorption sites in the cavities, specifically, at such a low xenon concentration, the primary interactions are expected with the metal nodes, as already observed for other gases such as argon[37,38] . When lowering the temperature, both the signals shift to higher chemical shifts, suggesting a stronger interaction with the walls of the host. Xenon is an intermediate element on the column of the periodic table with respect to the radioactive targeted noble gases (^{85}Kr and ^{222}Rn) under study, thus this

experiment, performed under a continuous flow of xenon and at room temperature, provides a direct demonstration of absorption of noble gas of the two frameworks.

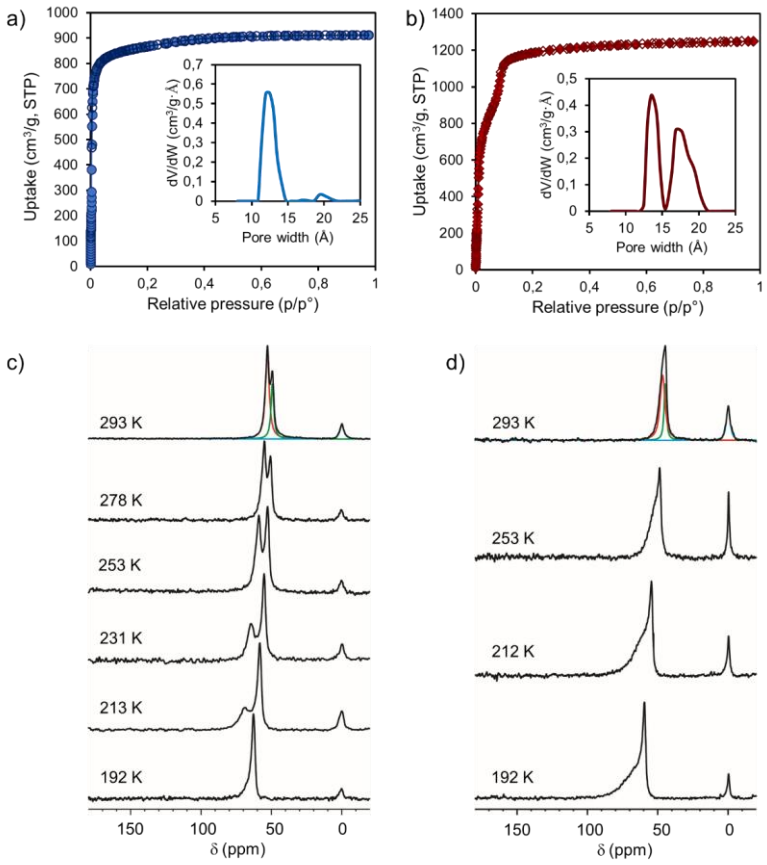

Figure 3 : N_2 adsorption isotherms at 77K of MOF-5-ADC (a) and MOF-205 (b). In the insets pore size distribution as calculated by Non Linear NL-DFT and carbon slit pores. CW-HP 129 Xe NMR spectra of MOF-5-ADC (d) and MOF-205 (e) as function of temperature. The peak at 0 ppm corresponds to the free Xe

Exposure to radioactive gas:

As mentioned above, our targets are ^{222}Rn, ^{85}Kr, and ^{3}H. Each gas has its own specificity, described in the introduction. ^{85}Kr was chosen as gas to screen the performance of all scintillating MOFs because it has a quasi-pure beta emission (99.7%) with relevant energy and a stable isotope daughter. As a first approach, this will give more signal than the low energy beta of the tritium and more ease of interpretation compared to the complex decay chain of the ^{222}Rn (ESI - Figure S1). It also has a lesser contamination potential than tritium; therefore, samples would be readily reusable for different test-

runs. Once the entire tests are completed, the sample is then used in the second test bench for tritium experiments.

^{85}Kr exposure:

^{85}Kr produces charged beta particles with a maximum energy of 687 keV; this implies the generation of Cherenkov light in the glass walls of our vials. The Cherenkov Effect is anisotropic, which makes it harder to detect by our set-up due to the geometry of our triple coincidence setup. Nevertheless, diffusion/reflection phenomenon can occur, and thus a background of Cherenkov light is observable when an empty vial is used in the system (ESI Figure S37). A very weak T/D indicator (ESI Figure S38) also characterizes the Cherenkov background, which is understandable from its anisotropic nature. This control procedure enables the evaluation of the real impact of subsequent loading with the samples.

The closest to a porous scintillator that we found in the literature are scintillating microspheres developed by Tarançon *et. al.* [39], which present the highest surface/volume ratio tested for solid scintillators. These microspheres also exhibit a small permeability toward gas[40] . We choose these scintillating microspheres as another point of reference and the experiments showed that their response is higher than the blank measurements, hence validating its use for the detection of radioactive gas.

For all the MOFs samples, the same experiments were performed as described in the method section, thus using a well-known activity concentration coming from the same activity standard. As mentioned, each MOF sample was activated by solvent exchange followed by a vacuum and temperature treatment. The MOFs were then stored in a glovebox before being characterized on the gas bench. Due to the exposition to nitrogen from the glovebox and the use of dry air as a carrier, we consider the pore of the MOFs already filled. Therefore, our working hypothesis relies on the diffusion and uptake of radioactive gas in the pores. Strong of numerous literature reports on MOFs selectivity[41] , we were also expecting other effects to influence the measurements:

- The first concerns the affinity of certain gases with certain MOFs, which concentrate the gas inside the MOFs, making a local increase of its concentration, and thus activity in case of a radioactive gas; this effect is labeled as a concentrator effect.
- The second is the difference in the diffusion dynamic of gas inside the porous architecture, which will dictate the dynamic of the system at the injection but also at the purging step with potential gas retention.

After injection and circulation of the radioactive gas, the system was allowed to reach equilibrium, corresponding to a plateau observed in the *D* count rate. Then the whole system was purged with the circulation of dry air.

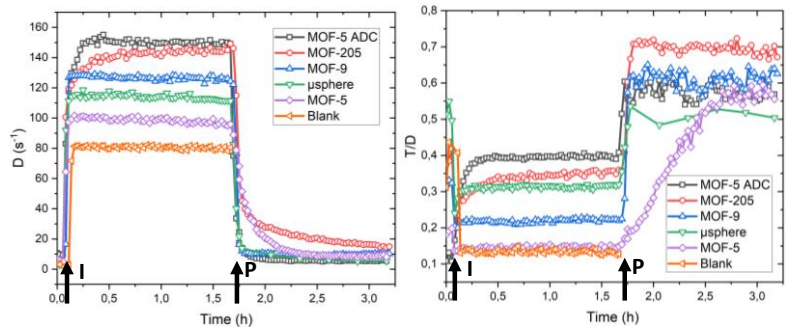

Figure 4: Left: Count rate of different substrates exposed to a ^{85}Kr atmosphere. Right: Associated TDCR yields. I = Injection of radioactive atmosphere P = Purge with dry air

As presented in Figure 4, all the tested MOFs presented a count rate superior to the blank, which indicates that more photons are detected than a pure Cherenkov effect. To ensure that the photons are coming from a scintillation mechanism, one last control is necessary here. One possibility is that our fluorescent MOF acts as a fluorescence shifter, absorbing the unidirectional Cherenkov emission and reemitting it isotropically at a longer wavelength better suited for the PMTs. This possibility was discarded with a control test of our best counting sample (MOF-5-ADC) but with the sample holder's cavity plugged. This experiment (ESI figure S36 S37 S38) produced the same counting rate and *T/D indicator* as the empty control experiments without a plug, showing that Cherenkov shifting is negligible in our systems. Thus it confirms that every count rate above the Cherenkov blank can be attributed to scintillation due to the interaction of the radioactive gas radiation with the MOFs samples. With this control experiment in mind, the results show that MOF-5 is worse than the reference scintillating microspheres, but that MOF-9, MOF-205 and MOF-5-ADC are increasingly better in term of count rate.

As stated before, the count rate is mainly dependent on the scintillation efficiency and its wavelength in regards to the optimal PMT quantum efficiency. Our best MOFs with the highest counting rate from this screening are MOF-205 and MOF-5-ADC. This is coherent as they are the two MOFs with the emission profile the closest to the PMT maximum efficiency (40 % between 280 nm and 420 nm). With the shorter TDCR coincidence window (40 ns), MOF-205 and MOF-5-ADC give *D* count rates of 170 s^{-1} and 200 s^{-1}, respectively when exposed to a flux of ^{85}Kr. This value can be subtracted from the Cherenkov blank to give us 70 s^{-1} and 100 s^{-1} from pure scintillation phenomena for our two best MOFs. With the volume of the sample holder, we can deduce a primary efficiency of detection for ^{85}Kr exposure.

$$\varepsilon_D = \frac{D}{A_V \times V} \quad \text{(EQ1)}$$

Where ε_D is the primary detection efficiency, *D* is the net count rate in s^{-1} (blank and Cherenkov count rate being deduced) observed on the average of the logical sum of the double coincidence plateau, A_V is the injected volumic activity in $s^{-1} \cdot cm^{-3}$, and *V* is the volume of the cavity in cm^{-3}. The ε_D values for the MOFs are represented in Table 2.

Table 2: Parameters and efficiency for MOF-205 and MOF-5-ADC

	Cps	A_v	V	ε_D (%)	ε_c (%)
MOF-205	70	74.6 $Bq \cdot cm^{-3}$	0.5 cm^3	188	207
MOF-5-ADC	100	75.7 $Bq \cdot cm^{-3}$	0.5 cm^3	264	334

These ε_D values are a first indicator of the performances of our samples and are already above 100 %. This is an evidence of an awaited concentration effect of our MOFs, meaning that ^{85}Kr would preferentially interact inside the pores, and have a local concentration inside the MOFs superior to the injected one.

The first approach to correct this ε_D efficiency is to estimate the true volume accessible to the gas since the MOF occupied a specific volume in the cavity as well as the true activity that interacts with the MOFs. Given that these two values are overestimated here, the primary efficiency presented here is a lower value of the system's true potential.

With the knowledge of the MOFs' mass we put inside the cavity (181 mg and 161 mg, respectively for MOF-205 and MOF-5-ADC) and the theoretical density of our MOFs (0.3 and 0.2)[42], we can evaluate the percentage of the occupied volume by MOF-205 and MOF-5-ADC at 47.6% and 40.0% respectively. As MOFs are porous architectures, this volume must be corrected by the percentage of the void present in these architectures. This correction was calculated using lattice parameters and experimental pore size, obtained by BET, to obtain a percentage of the MOF actually occupied by matter. The values are 21% and 52% for MOF-205 and MOF-5-ADC. This gives us a final volume occupied by the MOFs of 9.52% and 20.8%, respectively, percentages that need to be deduced to access the corrected volume (V_c).

We also performed MCNP-6 simulation to estimate the percentage of beta that interacts with our system. Our MOFs are not very dense, therefore, there is a possibility that beta escape and does not interact with our scintillating MOFs. The simulation provides us with a 99.7% proportion of beta that interact and deposit at least 1 keV inside the MOF. So only 0.3% of the beta from ^{85}Kr decay are not seen by our system and so the corrected volumetric activity (A_{Vc}) is comparable to the uncorrected one. This

With these corrected value V_c and A_{Vc}, we can infer a corrected efficiency that comes a little closer to the true efficiency of our system:

$$\varepsilon_c = \frac{D}{A_{Vc} \times V_c} \text{ (EQ2)}$$

These ε_c efficiencies are not yet true efficiency measurements as several parameters such as scintillation yields, transparency of the media, or nonlinearity of the scintillator are not consider. For example, in case of very low energy interaction, only a few photons will be emitted, so the probability of registering a coincidence event will diminish. These effects in the case of ^{85}Kr are negligible because of its beta spectrum that is relatively high, hence are not explored here.

This gave us efficiency of 207 % for MOF-205 and 334% for MOF5-ADC. Once again, efficiency over 100% is a notable thing that we expected and explain by the nature of the MOFs with their ability to interact favorably with the targeted gas, hence artificially concentrating it inside the MOFs. This concentration effect increases the number of radioactive atoms inside the pores of our MOFs and thus inflating the count rate and the efficiency of our system. This validates our hypothesis that MOFs porosity is a game-changer for noble gas low-level activity measurements.

The *D* count rate and the *T/D* indicator obtained with the MOFs were continuously observed (Figure 4) as the system was purged with dry air. The combined analysis of these two values gave us a strong indication of the capacity of our MOFs to trap the ^{85}Kr. The general analysis of a result can be broken down as follows:

1. First step: Baseline measurements before ^{85}Kr injection. The measurements give a low count rate due to external interactions (muons, natural radioactivity, …) in the scintillating material with a fluctuating but stable *T/D* value over time (fluctuation due to low statistics). This step is here to determine our baseline.

2. Second step: injection of ^{85}Kr, the *T/D* value changes in seconds after injection; it is generally different from the blank and depends on the detected radiation (low or high energy) and the scintillator (its scintillation yield including the light collection). In our case, the *T/D* just after injection quickly reaches a low value that is characteristic of the Cherenkov effect, and then increases slowly over 10 minutes due to the better yields of the scintillation process as it diffuse inside the scintillating MOF.

3. Third step: the ^{85}Kr has circulated in the loop, and the *T/D* and the count rate *D* reaches a horizontal plateau. The *T/D* comes from both the scintillation of the MOF (good efficiency) and from the Cherenkov effect due to the high-energy charged particles interacting in the glass of the vials (low efficiency).

4. Fourth step: clean air is circulated into the loop; the *T/D* value increases because ^{85}Kr that is not trapped in the MOF is removed, so the Cherenkov effect disappears and the photons comes from the scintillating MOF directly (higher efficiency). If the count rate *D* decreases slowly at the same time, this means that a dynamic of desorption is observable and that it comes from the MOF itself.

5. Last step: after a long air cleaning process, if *T/D* is maximum and the *D* count rate is higher than the blank, this means that a small amount is trapped into the material and that we are measuring the scintillation from the MOF. On the contrary, if the *T/D* and *D* come back to a similar value to that of step one, the radioactive gas has spread out, and the MOF is back to normal.

As shown in Figure 4, some MOFs released their load in a few seconds whereas others exhibited a slower dynamic of desorption. MOF-5 exhibits the slowest desorption. The case of MOF-205 is also interesting as it shows a mixed desorption dynamic with at first a rapid decrease of the counting rate, but reaching a very shallow slope that indicates remaining but unknown quantity of ^{85}Kr strongly adsorbed inside the MOFs. This can be interpreted since the MOF-205 has two sizes of pores inside its lattice 13.5 Å and 17.3 Å. The smallest one could be responsible for this particularly long desorption process.

The study of the count rate during the purge is also fascinating as we expect a quasi-instantaneous purging of the volume not occupied by the MOF sample, thus extinguishing all Cherenkov contribution. As explained above, the Cherenkov effect is anisotropic and therefore has a very poor *T/D* indicator evaluated at 0.15 in the control experiment (Figure 4 blank). During the plateau, the measurements of the *T/D* indicator are a combination of both Cherenkov radiation and scintillation from the MOF. This *T/D* value was evaluated at only 0.35 for both MOF-205 and MOF-5-ADC. Once the Cherenkov effect is extinguished by purging with dry air, we found ourselves only with the scintillation contribution from the MOF and an increased *T/D* indicator of 0.72 for MOF-205 and 0.55 for MOF-5-ADC. This high *T/D* is another testimony of the potency of MOFs as scintillators. To explore our system's potential, we performed a series of experiments with ^{85}Kr.

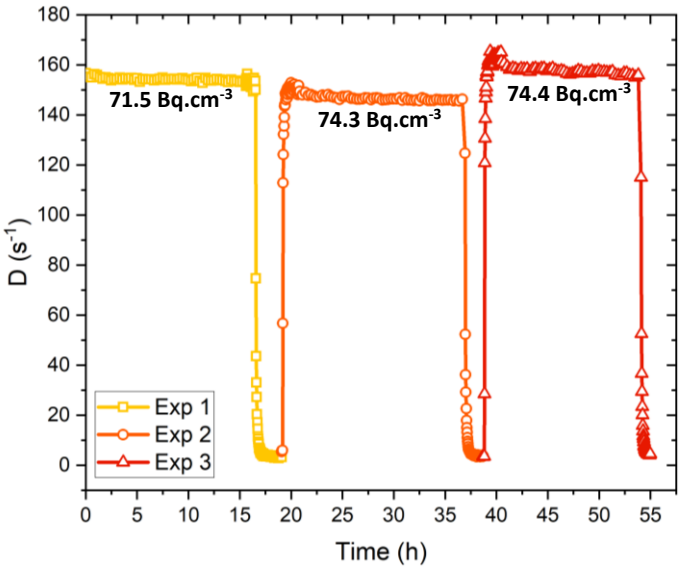

Figure 5: Count rate reproducibility and long-time exposure experiments of MOF-205 against ^{85}Kr.

In Figure 5 we demonstrated the reproducibility of the measurements. Three active atmospheres of around 10 kBq were loaded in succession with intermediate purging of the system and with the same MOF-205 sample inside. The exact activity of each active load was previously measured and then compared to the count rate. The variation of the counting rate from these three measurements corrected by the activity gives us a first evaluation of the reproducibility of the response of the sample with a standard deviation of X% .

Commenté [BG4]: @ sharvanee pour la stat

Our next step was to determine the response of our system towards different activities. In this endeavor, we used the full range of activity our test bench could make for a sample which is from 5 kBq to 0 kBq per samples. If we consider the volume of our system, this is equivalent to 35 Bq·cm^{-3} – 280 Bq·cm^{-3}. The results of these experiments are shown in Figure 6. We can extract two major key pieces of information from this study. First, if we plot the plateau average against the injected activity (Figure 6 right), we obtain the response function of our system and we can analyze the linearity of our results. On the experimented range, the system gives a remarkable linearity, which is another advantage to our approach. This also shows that the MOF-205 response is not saturated in this range. Nonlinearity is expected at higher injected activity but 280 Bq.cm^{-3} is the upper limit of our ^{85}Kr source generation . On the other side of this range, we can see that there is a lot of signal at low activity (35 Bq·cm^{-3}), but we were unable to make measurements below this level. This will be a particular focus in the future, as it will reached level compatible with the hardest industrial regulation (detection limit at 1 Bq·cm^{-3}).

Commenté [mha5]: Du coup il manque dans la figure la valeur 40 kBq, ou alors il faut changer le wording de la limite d'utilisation à 35 kBq

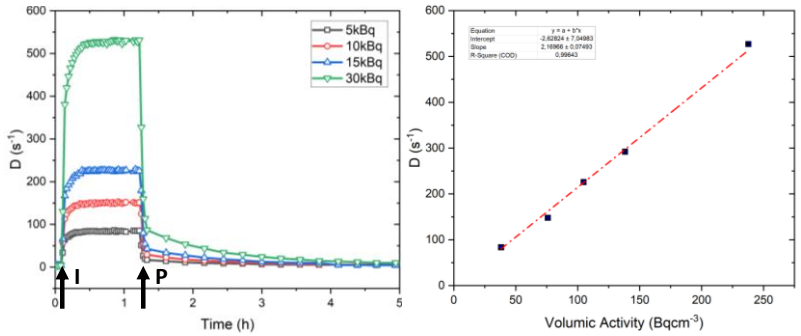

Figure 6: Left: Count rate given by MOF-205 when exposed to atmosphere with different activities of ^{85}Kr. Right: average count rate of the plateau plotted against the injected activity and the associated linear fit. I = Injection of Radioactive Atmosphere P = Purge with dry air

Commenté [mha6]: À droite il manque un point entre Bq et cm-3 dans le titre de l'abscisse

^{222}Rn exposure:

The same setup configuration was used to test our two best MOFs with ^{222}Rn (MOF-205 and MOF-5-ADC, Figure 7). The decay chain of ^{222}Rn contains 3 alpha and 2 beta emitters at the equilibrium considering the ^{210}Pb as stable due to its long half-life (of 22.23 years) compared to our experiment's time (up to 3 days) (ESI Figure S1). The total interpretation of the response with radon is however complicated due to the fact that its decay products are solid isotopes of lead, bismuth, and polonium, so they act differently compared to gases. The decay data from the Decay Data Evaluation Project[43] allows us to calculate a secular equilibrium time of 4 h. These two pieces of information are relevant, as they will set a minimum exposition time of 4 h in order to have a stable repartition of the different emitters' contributions inside the MOF.

Following our methodology for ^{85}Kr, we also performed here a blank measurement without MOFs and a measurement with scintillating plastic microspheres. The first blank is here to evaluate the Cherenkov contribution of the beta but also the photoluminescence possibility of N_2 excited by alpha particles. This "air" component of our system is taken into account and presented in Figure 7 - blank. This shows a maximum *D* count rate of 3800 s^{-1} at 4 h, which corresponds to the secular equilibrium of ^{222}Rn. This is followed by a steady decrease in the count rate that can be attributed to the decay of ^{222}Rn and its decay products. The *T/D* ratio for these measurements is relatively high, 0.53, compared to the one of ^{85}Kr experiments (Figure 4). This implies a small contribution of Cherenkov and a majority of detected events from the N_2 luminescence. The control experiment with scintillating microspheres showed a slightly lower count rate but higher *T/D* indicator. We attribute the lower count rate to highly diffusive behavior of the microsphere which tends to favor optical self-adsorption and thus diminishes the effective light output. The filling factor of the microspheres that slightly reduces the volume available to the gas could also explain a lower total activity of radioactive gas in the chamber hence a lower count rate. Nonetheless, the higher T/D indicator (ESI Figure SXX) showed that efficient scintillation phenomena are occurring. This is also valid for our two MOFs, which exhibit strong response due to scintillation, that double the count rate compared to the blank.

Furthermore, the relatively short lifetime of the ^{222}Rn can also be observed in our system, which confirms the observation of the targeted gas. A longer experiment (Figure 8) was performed and gave

us a half-life of Radon of 3.7995 days. This value is 0.62% away from the official one: 3.8232 days[44], but it is the first time such a half-life is measured using a solid porous medium.

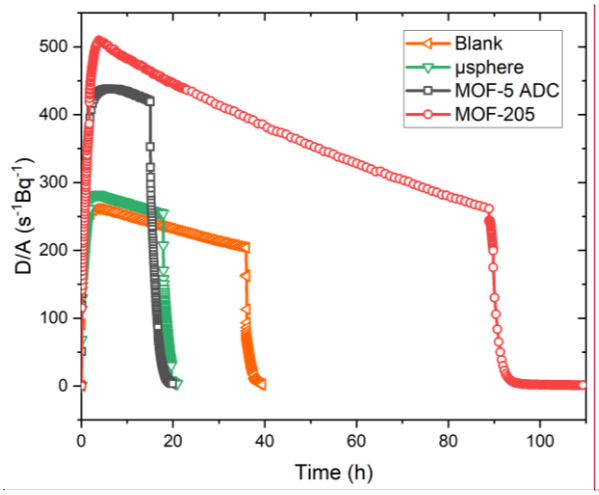

Figure 7: Count rate of different substrates exposed to an atmosphere of ^{222}Rn. I = Injection of radioactive atmosphere; P = Purge with dry air

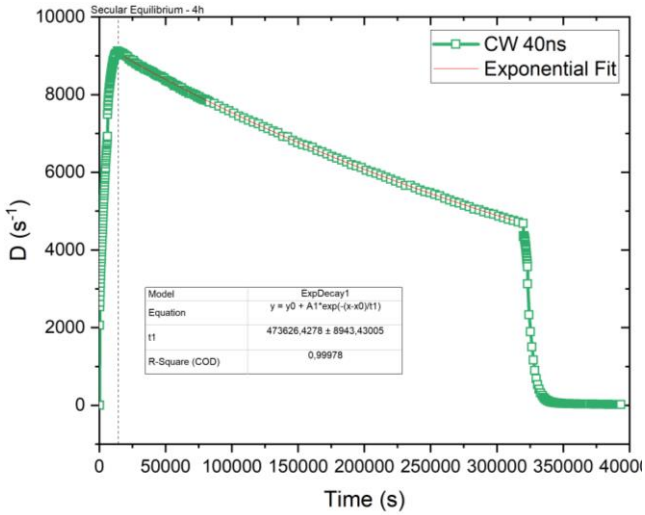

Figure 8: MOF-205 count rate evolution in regard of time during long exposure to ^{222}Rn and the associated exponential fit for the half life measurments of ^{222}Rn. The doted line at 4 hour represent the secular equilibrium.

Tritiated dihydrogen Exposure:

Commenté [BG7]: @ sharvanee un graph avec les rendements TDCR homogène je les mettrais en SI ou à côté.

Commenté [mha8]: Encore une fois, nommer les mof en fonction des codes couleur

Commenté [VV9]: De la même manière qu'en bas, rajouter une ligne vertical à 4h pour montrer l'ES

Commenté [VV10]: On est pas homogène sur l'abscisse. A mettre en h

Tritium is the most challenging radioelement to test in our system, as it contaminates the entire piping and requires extensive cleaning post-measurement to avoid contamination of the following measurement, as well as accidental release. To mitigate such problems, we are working here with HT gas inside pure nitrogen. Furthermore, tritium's beta decay has a very low energy (average 5.7 keV, max 18.6 keV), hence generating very few photons for each interaction. So far, with the best liquid scintillator (e.g. toluene containing 2,5-diphenyloxazole (PPO) and 1,4-bis(5-phenyloxazol-2-yl) benzene (POPOP)) mixed with organic tritiated compound, the TDCR device we use gives a maximum of 0.76 for the *T/D* indicator in comparison to 0.54 with a commercial scintillator and tritiated water[45] . However, even for low energy, the detection efficiency is not negligible as we are set to unique photon detection with the TDCR device. This is where the choice of TDCR measurements shines: we can reliably say that slight variations in the count rate are significant and not statistical errors. Here also, MOF-205 and MOF-5-ADC were tested and compared to a blank experiment (Figure 9). As tritium is a pure, low-energy beta emitter, neither Cherenkov nor air contribution are awaited. As expected, the blank counting rate did not change upon injection of 70 kBq.cm^{-3} of the radioactive gas. But for MOF-205 and MOF-5-ADC, an increase of 2.02 cps and 0.99 cps were respectively observed. Upon purging, the count rate came back to its initial value, showing no observable adsorption of the tritium inside the MOFs. If we compare those count rates with the activity present inside the sample cavity (0.5 cm^3) we can deduce a detection efficiency for MOF-205 and MOF-5 ADC which are respectively 5.8% and 2.8%. This value seems to be low in comparison with liquid scintillation (40 - 50 % efficiency)[46,47] but it is relatively on par with diffusion chamber (5 - 14 % efficiency)[48].

As opposed to ^{85}Kr and ^{222}Rn, the detection of tritium is very weak in terms of count-rate, but nevertheless successful. We are still far away from the efficiency of liquid scintillation, but one can note the rapid response time of our system, which is in the range of minutes. This is a remarkable achievement considering the length of traditional measurements, which make tritium often considered as the most difficult commonly occurring radioisotope to measure.

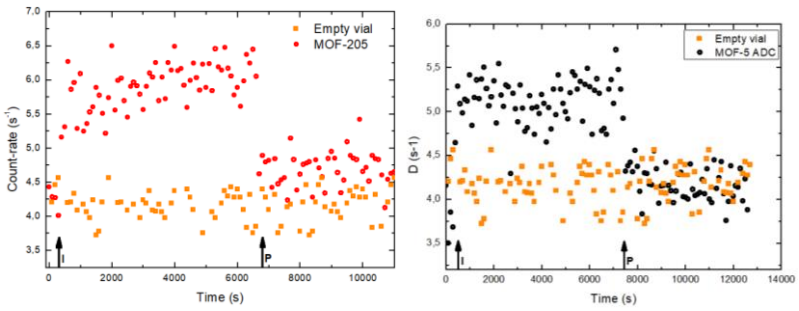

Figure 9: Count rate of MOF-205 (left) and MOF-5-ADC (right) when exposed to HT. I = Injection of radioactive atmosphere P = Purge with dry air

Commenté [VV11]: Homogénéiser taille et légende ordonnée des figures

Conclusion

Following previous reports in the literature that used MOFs as scintillators embedded in plastic matrices, we demonstrate here that fluorescent MOFs are a very potent solution for the detection of radioactive gas. This dual approach, using MOFs as both scintillators and gas sponges, was built on screening several candidates on a unique TDCR setup that allowed us to manipulate various radioactive gases. This enables us to test the three most important radioactive gases in terms of society impact (^{85}Kr, ^{222}Rn, and hard-to-detect ^{3}H). The first screening put forward two candidates as efficient scintillators: MOF-205 and MOF-5-ADC. These two MOFs were then extensively characterized by solid-

state and xenon NMR. These samples were tested extensively on ^{85}Kr and demonstrated a remarkable reproducibility and linearity of response. Furthermore, their high efficiency justifies our hypothesis of a concentration effect inside the MOFs. As ^{85}Kr represents the majority of the manmade emission, our system would already be the only online detection solution able to follow its emission from a reprocessing nuclear fuel plant chimney. MOF-205 and MOF-5-ADC also gave successful results for the detection of ^{222}Rn with the observation of its half-life. Finally yet importantly, tritiated dihydrogen was also counted with our scintillating MOFs. These breakthrough results validate our approach and pave the way towards a new paradigm in the detection of radioactive gas with porous scintillators and, hopefully, a breakthrough in their controlled emissions.

Acknowledgements

This project has received funding from the European Union's Horizon 2020 research and innovation program under grant agreement no. 899293. This document reflects only the authors' view and the Commission is not responsible for any use that may be made or the information it contains.

Sergio Piva is acknowledged for his contribution to HP Xe NMR experiments.

Competing interests

The authors declare no conflict of interest

Additional information

Original data and electronic supplementary information available upon request.

Bibliography

1. Mamuro, T., Fujita, A., Matsunami, T., Yoshikawa, K. & Azuma, T. Radioactive air-born dust in japan. *Nature* **194**, 643–644 (1962).
2. Measday, D. F. & Ho, E. C. Y. Experience with a prototype of the Test Ban Treaty monitoring system for air-borne radioactivity. in *Nuclear Instruments and Methods in Physics Research, Section B: Beam Interactions with Materials and Atoms* vol. 213 464–468 (2004).
3. Hou, X. Liquid scintillation counting for determination of radionuclides in environmental and nuclear application. *Journal of Radioanalytical and Nuclear Chemistry* vol. 318 1597–1628 Preprint at https://doi.org/10.1007/s10967-018-6258-6 (2018).
4. Varlam, C., Stefanescu, I., Duliu, O. G., Faurescu, I. & Popescu, I. Applying direct liquid scintillation counting to low level tritium measurement. *Applied Radiation and Isotopes* **67**, 812–816 (2009).
5. Tuo, X., Mu, K., Li, Z. & Li, X. Tritium monitor based on gas-flow proportional counter. in *Journal of Nuclear Science and Technology* vol. 45 171–174 (Taylor and Francis Ltd., 2008).
6. Orano group. *Orano Cycle Rapport d'information du site de la Hague*. https://www.orano.group/docs/default-source/orano-doc/groupe/publications-reference/rapport-tsn-la-hague-2019.pdf (2019).

7. Ahlswede, J., Hebel, S., Ross, J. O., Schoetter, R. & Kalinowski, M. B. Update and improvement of the global krypton-85 emission inventory. *J Environ Radioact* **115**, 34–42 (2013).

8. European commission. *EUR-Lex - 31996L0029*. *European directive 31996L0029* (1996).

9. Thomas B. Borak & Janet A. Johnson. *Estimating the Risk of Lung Cancer from Inhalation of Radon Daughters Indoors Review and Evaluation*. (1988).

10. Philippe, P. & Dafina, D. *RADON LEVELS IN DWELLINGS*. www.euro.who.int/ENHIS (2019).

11. Surette, R. A. & Mcelroy, R. G. C. *A REVIEW OF TRITIUM-IN-WATER MONITORS*. (1986).

12. Theodorsson, P. A review of low-level tritium systems and sensitivity requirements. *Applied Radiation and Isotopes* **50**, 311–316 (1997).

13. Odziomek, M. *et al.* Design and Application of High Optical Quality YAG:Ce Nanocrystal-Loaded Silica Aerogels. *ACS Appl Mater Interfaces* **10**, 32304–32312 (2018).

14. Kreno, L. E. *et al.* Metal-organic framework materials as chemical sensors. *Chemical Reviews* vol. 112 1105–1125 Preprint at https://doi.org/10.1021/cr200324t (2012).

15. Wang, C. *et al.* Synergistic assembly of heavy metal clusters and luminescent organic bridging ligands in metal-organic frameworks for highly efficient X-ray scintillation. *J Am Chem Soc* **136**, 6171–6174 (2014).

16. Feng, P. L. *et al.* Designing metal-organic frameworks for radiation detection. in *Nuclear Instruments and Methods in Physics Research, Section A: Accelerators, Spectrometers, Detectors and Associated Equipment* vol. 652 295–298 (2011).

17. Perego, J. *et al.* Composite fast scintillators based on high-Z fluorescent metal–organic framework nanocrystals. *Nat Photonics* **15**, 393–400 (2021).

18. Perego, J. *et al.* Highly luminescent scintillating hetero-ligand MOF nanocrystals with engineered Stokes shift for photonic applications. *Nat Commun* **13**, (2022).

19. Perry Iv, J. J. *et al.* Connecting structure with function in metal-organic frameworks to design novel photo- and radioluminescent materials. *J Mater Chem* **22**, 10235–10248 (2012).

20. Villemot, V. *et al.* From Sintering to Particle Discrimination: New Opportunities in Metal–Organic Frameworks Scintillators. *Adv Photonics Res* **3**, 2100259 (2022).

21. Sabot, B., Dutsov, C., Cassette, P. & Mitev, K. Performance of portable TDCR systems developed at LNE-LNHB. *Nucl Instrum Methods Phys Res A* **1034**, (2022).

22. Sabot, B., Rodrigues, M. & Pierre, S. Experimental facility for the production of reference atmosphere of radioactive gases (Rn, Xe, Kr, and H isotopes). *Applied Radiation and Isotopes* **155**, (2020).

23. Sabot, B., Pierre, S. & Cassette, P. An absolute radon 222 activity measurement system at LNE-LNHB. *Applied Radiation and Isotopes* **118**, 167–174 (2016).

24. Broda, R., Cassette, P. & Kossert, K. Radionuclide metrology using liquid scintillation counting. *Metrologia* **44**, (2007).

25. Sabot, B., Dutsov, C., Cassette, P. & Mitev, K. Performance of portable TDCR systems developed at LNE-LNHB. *Nucl Instrum Methods Phys Res A* **1034**, (2022).

26. Leith, G. A. *et al.* Confinement-guided photophysics in MOFs, COFs, and cages. *Chemical Society Reviews* vol. 50 4382–4410 Preprint at https://doi.org/10.1039/d0cs01519a (2021).

27. Stavila, V., Talin, A. A. & Allendorf, M. D. MOF-based electronic and opto-electronic devices. *Chemical Society Reviews* vol. 43 5994–6010 Preprint at https://doi.org/10.1039/c4cs00096j (2014).

28. Martin, C. R. *et al.* Let the light be a guide: Chromophore communication in metal-organic frameworks. *Nano Research* vol. 14 338–354 Preprint at https://doi.org/10.1007/s12274-020-3017-0 (2021).

29. Bertrand, G. H. v., Sguerra, F. & Hamel, M. Current status on plastic scintillators modifications. *Chem. Eur. J.* **20**, 15660–15685 (2014).

30. Bertrand, G. H. V., Hamel, M., Normand, S. & Sguerra, F. Pulse shape discrimination between (fast or thermal) neutrons and gamma rays with plastic scintillators: State of the art. *NIMPR-A* **776**, 114–128 (2015).

31. Villemot, V., Hamel, M., Pansu, R. B., Leray, I. & Bertrand, G. H. V. Unravelling the true MOF-5 luminescence. *RSC Adv* **10**, 18418–18422 (2020).

32. Pullen, S. & Clever, G. H. Mixed-Ligand Metal-Organic Frameworks and Heteroleptic Coordination Cages as Multifunctional Scaffolds - A Comparison. *Acc Chem Res* **51**, 3052–3064 (2018).

33. H. Furukawa *et al.* Ultrahigh Porosity inMetal-Organic Frameworks. *Science (1979)* **329**, 424–428 (2010).

34. Kaye, S. S., Dailly, A., Yaghi, O. M. & Long, J. R. Impact of preparation and handling on the hydrogen storage properties of Zn4O(1,4-benzenedicarboxylate)3 (MOF-5). *J Am Chem Soc* **129**, 14176–14177 (2007).

35. Comotti, A., Bracco, S., Valsesia, P., Ferretti, L. & Sozzani, P. 2D multinuclear NMR, hyperpolarized xenon and gas storage in organosilica nanochannels with crystalline order in the walls. *J Am Chem Soc* **129**, 8566–8576 (2007).

36. Comotti, A. *et al.* A single-crystal imprints macroscopic orientation on xenon atoms. *Chemical Communications* 350–352 (2007) doi:10.1039/b612002d.

37. Pawsey, S. *et al.* Hyperpolarized 129Xe nuclear magnetic resonance studies of isoreticular metal-organic frameworks. *Journal of Physical Chemistry C* **111**, 6060–6067 (2007).

38. Li, H., Eddaoudi, M., O'Keeffe, M. & Yaghi, O. M. Design and synthesis of an exceptionally stable and highly porous metal- organic framework. *Nature* **402**, 276–279 (1999).

39. Santiago, L. M., Bagán, H., Tarancón, A. & Garcia, J. F. Synthesis of plastic scintillation microspheres: Evaluation of scintillators. *Nucl Instrum Methods Phys Res A* **698**, 106–116 (2013).

40. Mitev, K. *et al.* Pilot Study of the Application of Plastic Scintillation Microspheres to Rn-222 Detection and Measurement. *IEEE Trans Nucl Sci* **63**, 1209–1217 (2016).

41. Banerjee, D. *et al.* Potential of metal-organic frameworks for separation of xenon and krypton. *Acc Chem Res* **48**, 211–219 (2015).

42. Sim, J. *et al.* Gas adsorption properties of highly porous metal–organic frameworks containing functionalized naphthalene dicarboxylate linkers. *Journal of the Chemical Society. Dalton Transactions* **43**, 18017–18024 (2014).

43. Kellett, M. A. & Bersillon, O. The Decay Data Evaluation Project (DDEP) and the JEFF-3.3 radioactive decay data library: Combining international collaborative efforts on evaluated decay data. in *EPJ Web of Conferences* vol. 146 (EDP Sciences, 2017).

44. CEA/LNE-LNHB /V. Chisté, M. M. B. LNE-LNHB/CEA-Table de Radionucléides. http://www.lnhb.fr/nuclides/Rn-222_tables.pdf (2010).

45. Sabot, B., Dutsov, C., Cassette, P. & Mitev, K. Performance of portable TDCR systems developed at LNE-LNHB. *Nucl Instrum Methods Phys Res A* **1034**, (2022).

46. Royal. H. BENSON & Robert L. MAUTE. Liquid Scintillation Counting of Tritium improvements in sensitivity by efficient light collection. *Anal Chem* **34**, 1122–1124 (1962).

47. Chapon, A., Pigrée, G., Putmans, V. & Rogel, G. Optimization of liquid scintillation measurements applied to smears and aqueous samples collected in industrial environments. *Results Phys* **6**, 50–58 (2016).

48. Aoyama, T., Sugiura, H. & Watanabe, T. *APPLICATION OF AIR PROPORTIONAL COUNTERS TO A TRITIUM-IN-AIR MONITOR*. *Nuclear Instruments and Methods in Physics Research* vol. 254 (1987).